Instability in the quantum restart problem

Ruoyu Yin, Qingyuan Wang, and Eli Barkai
Department of Physics, Institute of Nanotechnology and Advanced Materials, Bar Ilan University, Ramat-Gan 52900, Israel

(Received 24 May 2024; accepted 6 June 2024; published 24 June 2024)

Repeatedly monitored quantum walks with a rate $1/\tau$ yield discrete-time trajectories which are inherently random. With these paths the first-hitting time with sharp restart is studied. We find an instability in the optimal mean hitting time, which is not found in the corresponding classical random-walk process. This instability implies that a small change in parameters can lead to a rather large change of the optimal restart time. We show that the optimal restart time versus τ, as a control parameter, exhibits sets of staircases and plunges. The plunges, are due to the mentioned instability, which in turn is related to the quantum oscillations of the first-hitting time probability, in the absence of restarts. Furthermore, we prove that there are only two patterns of staircase structures, dependent on the parity of the distance between the target and the source in units of lattice constant. The global minimum of the hitting time is controlled not only by the restart time, as in classical problems, but also by the sampling time τ. We provide numerical evidence that this global minimum occurs for the τ minimizing the mean hitting time, given restarts taking place after each measurement. Last, we numerically show that the instability found in this work is relatively robust against stochastic perturbations in the sampling time τ.

DOI: 10.1103/PhysRevE.109.064150

I. INTRODUCTION

Random search processes might be sent by chance to an undesired course away from a preset target position or area of space. In such cases, the strategy of restart can be employed to tackle the decision-making conundrum of continuation or abortion of the process. This idea is modeled as stochastic processes under restart [1,2]. Since the early 2010s, the introduction of restart has opened a rapidly expanding research field, and related topics including the optimization of first-passage time, nonequilibrium steady states, etc., have further propelled the expansion of this field [1–32].

A general motivation for considering quantum dynamics with restart [33–44] is search processes using quantum computers (e.g., see Refs. [45,46]). More specifically, the first-passage time in random walks, defined as the time it takes a random walker to reach a target or threshold for the first time [47], characterizes the efficiency of a classical search. Probably the most studied examples are the first-passage time of a Brownian motion or a random walker on the line. For unbiased random walk in unbounded space, with restarts, namely resetting a random walker to its initial site at some time t_r, the expected first-passage time exhibits one unique minimum [1,4]. As conveyed by the authors' previous publication (see Ref. [48]), completely different behaviors are found in the quantum world within the context of *deterministic* restarts (see definitions below). Employing repeated measurements or monitoring with a period τ at the preset target state, one can define the *quantum hitting time*, as the quantum counterpart of first-passage time, via the record of measurement outcomes (see details below). Using deterministic restarts, there appear multiple minima, instead of a sole minimum, of the mean hitting time under restart [48]. More remarkable is the periodical staircase structure of the optimal restart time, along with plunges or rises, which manifest a kind of instability, as a quantum signature in the restart framework. This is attributed to the existence of several minima in the expected hitting time. In Ref. [48] we treated this staircase structure, but only when the target is set at the initial state, i.e., the return case. Here in this paper, we will delve into the universality of staircase structures and accompanied instability for general choices of the target location. More profoundly, the staircase structure converges to a unique structure in the limit of rare measurements, namely the large-τ limit, depending only on the parity of the distance between the initial state and the target.

The process of restarts for monitored quantum walks can be implemented on quantum computers [49]. One may wonder, given the instabilities we find, whether small stochastic perturbations in the sampling times, lead to the wipe-out of novel quantum features. When does the noise destroy the quantum effects discussed in this paper? And does a small amount of noise severely affect our results? We will answer these queries towards the end of this paper.

Another natural question is how to find the global optimum with respect both to the restart time and the measurement period. Both these parameters are, at least in principle, control parameters, in the mentioned quantum computer experiments. In the classical world, the sampling time is of little concern, and one may try to detect the walker continuously. In the quantum case, due to the Zeno effect which typically inhibits detection, sampling cannot be performed continuously, and hence the sampling time becomes an important parameter. Therefore, in the quantum case, we have two control parameters, while typically in the classical restart problem, we minimize hitting times by changing the restart time only. With restarts the fast sampling leads to Zeno physics and very long mean hitting times, when the initial and target states are nonidentical. So clearly too-small τ or too-large τ are not optimal for the sake of fast search and similarly with respect to the restart time. The analysis for this global

optimization problem will be treated in the final stage of this paper.

This paper is structured as follows: We present in the first place the concept of quantum hitting time, or the first-detected-passage time (in the absence of restart), for a periodically monitored quantum walk (Sec. II) [50–58]. Then the mean hitting time with restart is provided in Sec. III, for the model of a tight-binding quantum walk on an infinite line. Further analysis for the optimization problem of the optimal restart time, exposing instabilities in the quantum restart problem, expounds the main results of the paper in Sec. IV. We check the robustness of our results to noise in Sec. V. The minimization of the mean hitting time, with respect to both the measurement period and the restart time, is studied in Sec. VI, namely we search for the global minimum of the mean hitting time. We close the paper with a summary and discussions. A brief summary of part of our results was recently presented in a Letter [48].

II. THE QUANTUM FIRST-HITTING TIME IN ABSENCE OF RESTART

We first introduce the quantum first-hitting time problem, which is based on the continuous-time quantum walk [59] but with repeated monitoring (measurements). The Hamiltonian we will employ in this paper is a tight-binding model of a single particle, sometimes called the walker, on an infinite line

$$H = -\gamma \sum_{x=-\infty}^{\infty} [|x\rangle\langle x+1| + |x+1\rangle\langle x|]. \tag{1}$$

Here γ is the hopping rate and set as 1 in what follows. This is a lattice walk [60], as the particle can occupy the integers denoted with the ket $|x\rangle$, and the hopping is to nearest neighbors only. The energy spectrum is $E(k) = -2\cos(k)$ in units of γ, and the eigenfunctions of H are $\psi_k(x) = e^{ikx}/\sqrt{2\pi}$ with $k \in [-\pi, \pi]$. Such tight-binding Hamiltonians are used extensively in condensed matter. Then the propagation of the quantum wave packet (in the absence of measurement) is described by the probability of finding the particle at state $|x_d\rangle$ starting from $|x_0\rangle$ (both are spatial states of the lattice), i.e.,

$$\begin{aligned} P(x_d, x_0, t) &= |\langle x_d||\psi(t)\rangle|^2 = |\langle x_d|\hat{U}(t)|x_0\rangle|^2 \\ &= |i^{|x_d-x_0|}J_{|x_d-x_0|}(2t)|^2 = J^2_{|x_d-x_0|}(2t), \end{aligned} \tag{2}$$

where $|\psi(t)\rangle$ is the solution to the Schrödinger equation for the Hamiltonian Eq. (1), $\hat{U}(t) = e^{-iHt}$ is the unitary operator with $\hbar$ set as 1 in what follows, and $J_n(x)$ is the Bessel function of the first kind. This is led by the cosine law of the dispersion relation $E(k)$ [54,55]. Hence the quantum walker's travel is ballistic [61–64] and vastly distinct from the Gaussian spreading of a classical walker on a similar lattice [47]. To determine the time when the particle arrives at some target for the first time, one cannot simply observe the "walking" process of a quantum particle, since according to Born's rule it "freezes" the particle at some eigenstate of the observable. This gives rise to a fundamental process and debatable problem known as time-of-arrival in quantum physics [65]. A way to solve this issue renders the framework of "monitoring" the (unitary) walking process built to define the quantum *first-detected-passage* time or first-hitting time, via some measurement protocol, within which the stroboscopic measurement protocol has been investigated in full detail [45,50–58]. The stroboscopic monitoring protocol states the following: a quantum walker is initially dispatched at a localized state $|x_0\rangle$ (source), and one attempts to measure the walker on the detected state $|x_d\rangle$ (target) at fixed times, $(\tau, 2\tau, 3\tau, \dots)$. In between the measurement attempts, the system undergoes free evolution dictated by the Schrödinger equation. We employ von Neumann (strong) measurement described by the projection $\hat{D} = |x_d\rangle\langle x_d|$, so the outcome of each measurement is yes (detection) or no (null detection) with probabilities determined by the Born rule. For the *first* hitting of the walker at the nth measurement attempt, the output of the experiment must be "no, no, no, no,..., yes," namely a final success at the nth attempt following previous $n-1$ failure, since the experiment is done once the walker hits the detector, i.e., a yes event is recorded. Each null detection acts as a wipe-out of the component of the wave function at the target [51,53,54]. We will explain the effects from the null detection below, which manifest themselves in the quantum renewal equation. Inherently, n is a random variable and is defined as the first-detected-passage time or hitting time (in units of τ). We denote the amplitude of finding the walker for the *first* time at the nth attempt by ϕ_n [53]. Using the quantum renewal equation, one can in principle solve for the quantum first-hitting amplitude [54]:

$$\phi_n(x_d, x_0) = \langle x_d|\hat{U}(n\tau)|x_0\rangle - \sum_{m=1}^{n-1} \langle x_d|\hat{U}[(n-m)\tau]|x_d\rangle\phi_m. \tag{3}$$

Technically one uses Eq. (2) and iterations to solve this equation or one may employ generating function techniques. For example, $\phi_1 = i^{|x_d-x_0|}J_{|x_d-x_0|}(2\tau)$, which is expected from basic quantum mechanics Eq. (2), while $\phi_2 = i^{|x_d-x_0|}[J_{|x_d-x_0|}(4\tau) - J_0(2\tau)J_{|x_d-x_0|}(2\tau)]$. Equation (3) is a quantum counterpart of the well-known classical renewal equation, which is discussed in Ref. [47]. From Eq. (3), one can readily find the essential effects from the repeated local measurement conditioned with null outcome: The first-hitting amplitude is indeed related to the measurement-free transition amplitude $\langle x_d|\hat{U}(n\tau)|x_0\rangle$, but the measurement-free return amplitude propagated from the *prior* first-hitting amplitude, $\langle x_d|\hat{U}[(n-m)\tau]|x_d\rangle\phi_m$ $(m < n)$, should be subtracted, since they represent the events that have been aborted by the null detection from the statistical ensemble.

Using Eq. (3), one then finds F_n, the first-hitting probability at time n,

$$F_n = |\phi_n|^2. \tag{4}$$

With Eq. (2) and $\delta := |x_d - x_0|$, that denotes the distance between the source and target in units of the lattice constant, one obtains, via iterations [54]:

$$\begin{aligned} F_1 &= |\phi_1|^2 = J_\delta^2(2\tau), \\ F_2 &= [J_\delta(4\tau) - J_0(2\tau)J_\delta(2\tau)]^2, \\ F_3 &= \big[J_\delta(6\tau) - J_0(4\tau)J_\delta(2\tau) - J_0(2\tau)J_\delta(4\tau) \\ &\quad + J_0^2(2\tau)J_\delta(2\tau)\big]^2, \\ &\vdots \end{aligned} \tag{5}$$

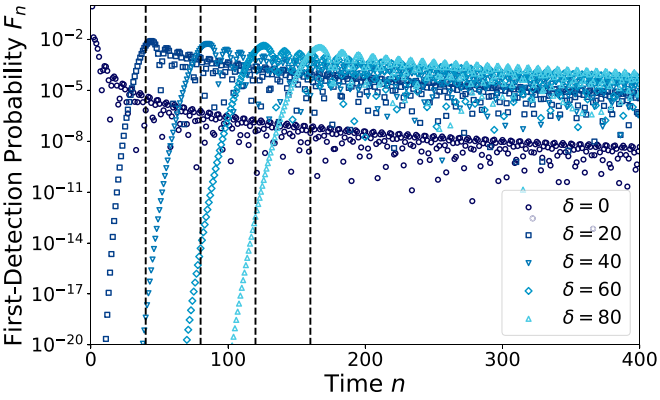

FIG. 1. F_n vs n for different δ, with $\tau = 0.25$ ($\gamma = 1$ as mentioned). The dashed lines represent the $n_{\text{inc}} = \delta/2\tau$, close to the $\max(F_n)$. For a thorough discussion on the quantum first-hitting probability, see Ref. [55].

A numerical demonstration is presented in Fig. 1 for different values of δ. As one may witness in the figure, besides the oscillatory decays, the maximum of F_n plays the role of a transition point distinguishing a rapid growth and a slow decay of F_n. The dashed lines at $n = 40, 80, 120, 160$ (correspond to $\delta = 20, 40, 60, 80$) approximately point to the maxima, and those special values of n are given by the maximal group velocity $\max(v_g) = \max[|\partial_k E(k)|] = 2$, the distance δ, and the measurement period τ in a kinematic fashion, $n_{\text{inc}} := \delta/2\tau$, hence we regard it as the "incidence" time of the ballistic-propagating wave front [55]. Around the n_{inc}, the chance for the detector to be hit reaches the maximum. Detailed analysis of F_n is provided in Refs. [54,55]. For a classical random walk, roughly speaking one has a peak in F_n that is determined by diffusive motion and the initial distance of target and source, followed by a power-law decay. In the quantum world nontrivial oscillations determined by a phase, superimpose on power-law decay are found [55]. Yet another difference between the classical and quantum hitting time problem is that the former is recurrent, while the latter is not, namely in general $\sum_{n=1}^{\infty} F_n < 1$ in the quantum case [50,66,67].

Now we will incorporate the restart framework with the quantum hitting time. As shown before, the ballistic propagation is a quantum advantage in faster search (over classical diffusive motion); however, as mentioned, F_n is unfortunately non-normalized in this 1D model (also in many finite systems), leading to infinite mean fitting times [50]. This indicates that the probabilistic nature of quantum dynamics sends the walker to undesired "trajectories" far away from the target or to the states orthogonal to the detected state in the Hilbert space *forever* [67]. A systematic strategy to solve this problem, inspired from processes happening in nature [68–70] or algorithmic methods used in classical computers [71,72], is to perform restarts to rescue a process that probably enters a wrong track. We expect the approach of restart to take advantage of the ballistic spreading of the wave front in each single *run* (one *run* is a monitored process between restarts), and in the mean time, to guarantee the detection of the quantum walker (see Appendix A), so that the quantum advantage of faster search is reinforced to pronounce the supremacy of the quantum search.

III. THE FIRST-HITTING STATISTICS UNDER RESTART

We will consider the deterministic restart (or sharp restart) strategy [7], namely after every r failed attempts in detecting the particle, the system is reset to the initial state to restart the monitored process. This strategy has been proven as the outperforming one, in the sense of unfailingly achieving the lowest minimum of the mean hitting time among all random restart strategies [3,10]. Let n_R be the first-hitting time under restart in units of τ. The general formula for the mean hitting time under sharp restart $\langle n_R(r)\rangle$ (the variable r means r steps between restarts) is

$$\langle n_R(r)\rangle = r\frac{1 - P_{\text{det}}^r}{P_{\text{det}}^r} + \langle n\rangle_{\text{cond}}^r, \tag{6}$$

where $P_{\text{det}}^r := \sum_{n=1}^r F_n$ is the detection probability within r attempts, and

$$\langle n\rangle_{\text{cond}}^r := \frac{\sum_{n=1}^r nF_n}{P_{\text{det}}^r}, \tag{7}$$

which computes the conditional mean of the first-hitting provided the particle is detected within r attempts. The F_n are the restart-free probabilities given with Eq. (5). This result has been presented in Refs. [3,73], and we also provide an alternative derivation in Appendix B. We note that in the large-r limit, for classical random walks in dimension one, $P_{\text{det}}^r \to 1$, then $\langle n_R(r)\rangle \to \langle n\rangle_{\text{cond}}^r$, while for the quantum walk Eq. (1), as mentioned above, $P_{\text{det}}^r \to \sum_{n=1}^{\infty} F_n < 1$. This implies that the first term in the right-hand side of Eq. (6), $r(1 - P_{\text{det}}^r)/P_{\text{det}}^r$, cannot be neglected in the large-r limit. We will show later that for the quantum walk on an infinite line, $\langle n_R(r)\rangle \sim ar + b$ when $r \to \infty$, with $a = (1 - P_{\text{det}}^{r=\infty})/P_{\text{det}}^{r=\infty}$, $b = \langle n\rangle_{\text{cond}}^{r=\infty}$, namely $\langle n\rangle_{\text{cond}}^r$ in the quantum case converges to a finite number.

In principle, substituting the first-hitting probability F_n Eq. (5) into the formula for the mean detection time under restart Eq. (6), we obtain $\langle n_R(r)\rangle$ for this specific model, an approach that is used to test the approximations studied below, the latter providing insights into the behaviors of the quantum restart. We provide a numerical demonstration of the general landscape of $\langle n_R(r)\rangle$ in Fig. 2. The first remarkable feature is the oscillations of $\langle n_R(r)\rangle$, leading to multiple extrema, which is vastly different from the classical restart with one distinct minimum [1]. Second, we notice that a small variation of the sampling time τ leads to a large change of the optimum, which switches in this example from $\langle n_R(6)\rangle = 19\,615$ to $\langle n_R(5)\rangle = 13\,287$. This suggests a type of instability as mentioned in the Introduction. Note the measurement periods τ's are chosen large here ($\tau = 150.10\pi$, 150.12π), which allows the application of asymptotic methods on our problem soon to be discussed.

More precisely, we list a few analytical expressions for $\langle n_R(r)\rangle$ using Eqs. (3), (5), and (6),

$$\langle n_R(1)\rangle = \frac{1}{F_1} = \frac{1}{J_\delta^2(2\tau)},$$

$$\langle n_R(2)\rangle = \frac{2 - F_1}{F_1 + F_2} = \frac{2 - J_\delta^2(2\tau)}{J_\delta^2(2\tau) + [J_\delta(4\tau) - J_0(2\tau)J_\delta(2\tau)]^2},$$

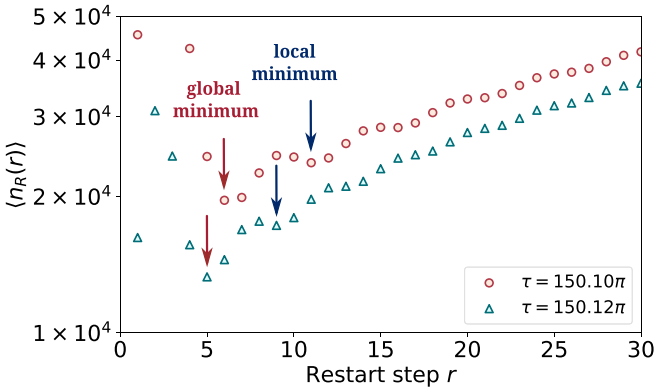

FIG. 2. The figure is changed according to referee's remarks. $\langle n_R(r)\rangle$ vs r for $\delta = 60$, with different τ. We see the oscillations of $\langle n_R(r)\rangle$ render the presence of several extrema (see the arrows), and the global minimum is located in small r, which will be analyzed below. When τ changes from 150.10π to 150.12π, we see a big change in the minimum of $\langle n_R(r)\rangle$, namely $\min\langle n_R(r)\rangle = 19\,615 \to 13\,287$, with the optimal restart step changing from 6 to 5. This shows that a slight change of τ causes a very large change of the optimum, indicating a type of instability.

$$\begin{aligned}\langle n_R(3)\rangle &= \frac{3-2F_1-F_2}{F_1+F_2+F_3}\\ &= \frac{3-2J_\delta^2(2\tau)-[J_\delta(4\tau)-J_0(2\tau)J_\delta(2\tau)]^2}{F_1+F_2+F_3},\\ \langle n_R(4)\rangle &= \frac{4-3F_1-2F_2-F_3}{F_1+F_2+F_3+F_4},\\ \langle n_R(5)\rangle &= \frac{5-4F_1-3F_2-2F_3-F_4}{F_1+F_2+F_3+F_4+F_5}, \quad \cdots . \end{aligned} \tag{8}$$

Those expressions are cumbersome; however, we will analyze particular limits where we may provide insights, e.g., large measurement period τ. In what follows, our discussions will be based on choosing certain values for δ to gain some insights (e.g., $\delta = 0, 1, 2, \ldots$) and investigating how to optimize the mean hitting time under restart. One of our goals is to find the optimal restart time r, denoted by r^*, which will be in general a function of τ and δ. The corresponding $\langle n_R(r^*)\rangle$ is then the optimal in the mean sense.

IV. OPTIMIZATION OF THE MEAN HITTING TIME

A. Return case: $\delta = 0$

We start with the "return" case where the detector is put at the origin to monitor the walker's first return, namely $\delta = 0$ [54]. We first consider the Zeno limit $\tau \to 0$. Specifically, in this limit, we have the following asymptotics for $\langle n_R(r)\rangle$ using Eq. (8):

$$\begin{aligned}&\langle n_R(1)\rangle \sim 1+2\tau^2, \quad \langle n_R(2)\rangle \sim 1+4\tau^2,\\ &\langle n_R(3)\rangle \sim 1+6\tau^2, \cdots . \end{aligned} \tag{9}$$

Clearly, the minimum is $\langle n_R(1)\rangle$. Hence the optimal restart $r^* = 1$ in the Zeno regime, and this is also intuitive, since the wave function is nearly frozen at the origin in the Zeno limit

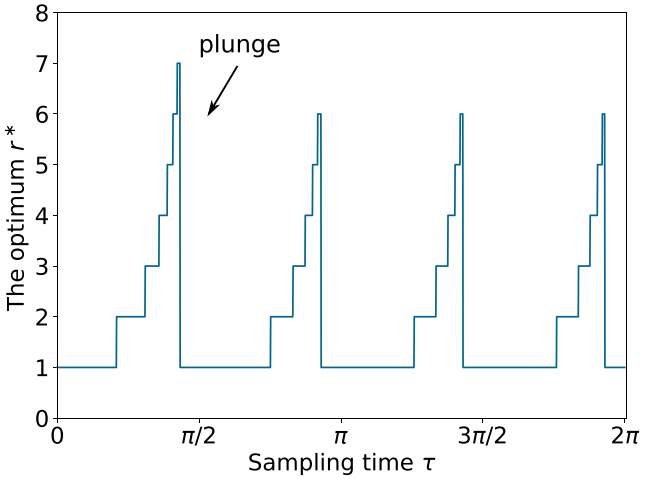

FIG. 3. The optimal restart time r^* as a function of τ for $\delta = 0$. We see the staircase structure accompanied by periodical plunges (see the arrow). As we increase τ we witness a convergence of the staircase structure.

[74], and it is always the best choice to restart after each failed measurement.

For large τ, with the large-x asymptotics for $J_n(x)$, namely $J_n(x) \sim \sqrt{2/\pi x}\cos(x - \pi n/2 - \pi/4)$ [75], we can re-express F_n for finite n as [54]

$$F_n(\tau) \sim \frac{1}{n\pi\tau}\cos^2\left(2n\tau - \frac{\pi}{4}\right). \tag{10}$$

In this limit there is a simple relation between the probability of first-hitting time and the measurement-free wave function. Namely, $F_n \sim P(0,0,t) = |\langle 0||\psi(t)\rangle|^2 = J_0^2(2t)$ with $t = n\tau$ and $|\psi(t)\rangle$ is the solution of the Schrödinger equation, in the absence of measurement, see Eq. (2). If 2τ is a multiple of π, then we find, using Eq. (10),

$$F_n \sim \frac{1}{2n\pi\tau}. \tag{11}$$

Thus, the restart-free F_n decays monotonically with n. For such a case, the best strategy of restart is to use $r = 1$, namely to restart after each measurement. We then have

$$r^* = 1, \quad \text{when} \quad 2\tau = k\pi, \tag{12}$$

where k is an integer. Using Eqs. (8,11), $\langle n_R(r^*)\rangle \sim 2\pi\tau$.

We now study how this optimal restart changes when we vary the sampling time τ, in particular, what is r^* as a function of τ? We have found that r^* exhibits a set of staircases, see Fig. 3. Clearly this behavior is far from the classical limit, and it is due to the oscillations of the first-hitting probability F_n. The optimal choice of r, presented in Fig. 3, is a periodical function of τ, with a period of $\pi/2$. Starting with $\tau = \pi k/2 \gg 1$, where k is an integer, when we increase τ slightly beyond this critical point, we find that $\langle n_R(1)\rangle$ is the optimal, i.e., the fastest approach to restart is still $r^* = 1$. We see transitions as τ is varied, from $r^* = 1$ to $r^* = 2$, and then to $r^* = 3$, etc., and finally a plunge to $r^* = 1$, and this is repeated. The staircase for small τ is not identical to that for large τ; however, as to be shown below in the latter limit,

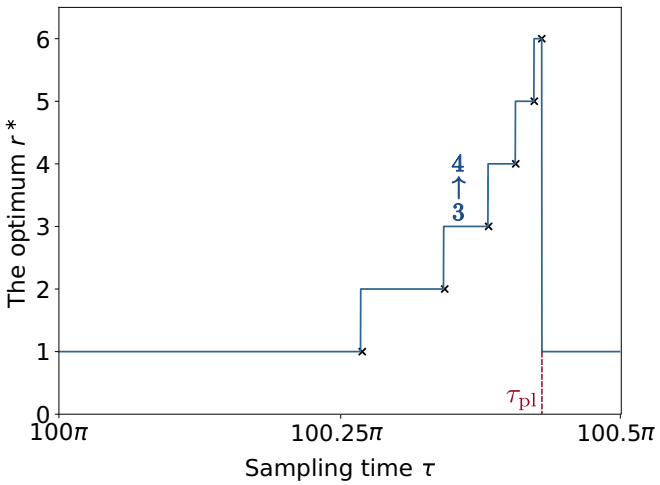

FIG. 4. r^* versus τ in the large-τ limit exhibits a limiting staircase and plunge. Here we use $\tau \in [100\pi, 100.5\pi]$ and $\delta = 0$. The cyan lines are the exact results, and the black crosses represent the approximations using Table I(a). $\tau_{\rm pl}$ here is approximated as $k\pi/2 + 1.353$ with $k = 200$.

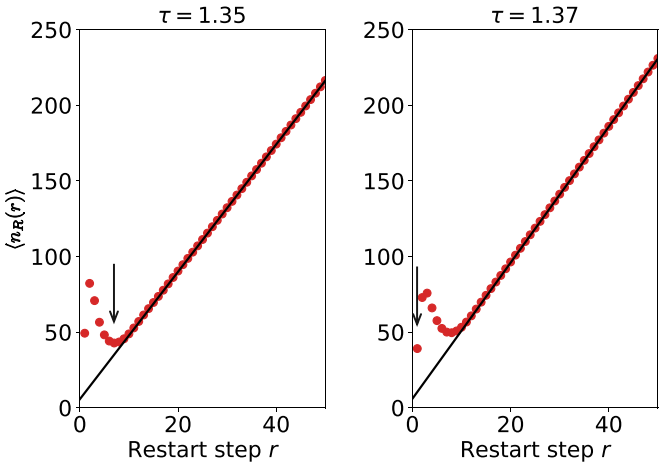

FIG. 5. $\langle n_R(r)\rangle$ vs r in the vicinity of the plunge τ ($\approx$1.36); see the drop of r^* ($7 \to 1$) at the leftmost staircase in Fig. 3. There are two minima competing with each other, and a small change of τ ($1.35 \to 1.37$) results in different optima. On the left panel $r^* = 7$ and on the right $r^* = 1$ (see the arrows). Thus a small change of τ creates a plunge of r^*. The solid lines represent the approximations to $\langle n_R(r)\rangle$ in the large-r limit, i.e., $\langle n_R(r)\rangle \sim r(1 - P_{\rm det}^{r=\infty})/P_{\rm det}^{r=\infty} + \langle n_R(\infty)\rangle_{\rm cond}$, where $\langle n_R(\infty)\rangle_{\rm cond} = \sum_{n=1}^{\infty} nF_n / \sum_{n=1}^{\infty} F_n$.

we will reach a particular pattern of staircases, presented in Fig. 4.

Now we also use the fact that $F_n \ll 1$ in the limit under study, namely the large-τ limit. Using Eq. (8), we find that the condition for τ, for the $r^* = 1$ to $r^* = 2$ transition, i.e., $\langle n_R(1)\rangle = \langle n_R(2)\rangle$, reads

$$F_1(\tau) = F_2(\tau), \tag{13}$$

and F_n are given in Eq. (10). We then find a sequence of transitions, and due to the fact that F_n is small, we find using Eq. (8), the transition $r^* = 2 \to r^* = 3$ at τ which solves

$$F_3(\tau) = [F_1(\tau) + F_2(\tau)]/2, \tag{14}$$

and similarly for the $r^* = 3 \to r^* = 4$ transition shown in Fig. 4,

$$F_4(\tau) = [F_1(\tau) + F_2(\tau) + F_3(\tau)]/3. \tag{15}$$

We see that the transitions are taking place when F_n is the mean of all the proceeding F_i's. At some stage these equations cannot be solved, in the sense that there is no τ giving a valid solution. We encountered already such a situation, and that is the Zeno limit. We can use Eq. (10) for $F_n(\tau)$ and find, with a simple computer program of calculation, the transitions in r^* at special sampling times.

Note that we have plunges where r^* falls to the value 1 (see the arrow in Fig. 3). In Fig. 5, we choose as an example two values of τ in the vicinity of $\tau \approx 1.36$. At this value we have a plunge (see Fig. 3). As shown in Fig. 5, there are two minima competing with each other, and the global minimum switches between them when τ is slightly varied. At the exact transition time τ for the plunge, the two minima are identical. Thus the system exhibits an instability in the sense that small changes of τ create large difference in the optimal restart time r^*.

We now calculate the sampling time $\tau_{\rm pl}$, where plunges are found. Let $\tau = k\pi/2 + \epsilon$ and $0 < \epsilon < \pi/2$. As mentioned in Eq. (12), if $\epsilon = 0$, then $r^* = 1$. We then denote $\epsilon_{1\to2}$ as the value of ϵ where we have a transition from $r^* = 1$ to $r^* = 2$, similarly for other transitions. In between the transition ϵ, namely for each interval $[\epsilon_{k\to k+1}, \epsilon_{k+1\to k+2}]$, we will check whether $\langle n_R(k+1)\rangle$ remains the minimum and especially compare it with $\langle n_R(1)\rangle$ in case we miss the plunge to $r^* = 1$. With Eq. (10) and Eqs. (13)–(15) we get Table I(a), which gives the values or ϵ for the various transitions, and check the minimum in Table I(b). Note that for the transitions with large r^*, ϵ is accumulating close to $\pi/2$, and hence the plateaus in optimal r are very small. Furthermore, when $1.353 < \epsilon < \pi/2$, r^* drops to 1, i.e., a sudden plunge as mentioned. So we

TABLE I. The ϵ at the transitions of r^* for $\delta = 0$.

(a) The values of $\epsilon_{k\to k+1}$.

$\epsilon_{k\to k+1}$	$\epsilon_{1\to2}$	$\epsilon_{2\to3}$	$\epsilon_{3\to4}$	$\epsilon_{4\to5}$	$\epsilon_{5\to6}$	$\epsilon_{\rm pl}$
Value	0.850	1.081	1.204	1.280	1.332	1.353

(b) The relation between $\langle n_R(k)\rangle$ and $\langle n_R(1)\rangle$ in $[\epsilon_{k-1\to k}, \epsilon_{k\to k+1}]$.

$[\epsilon_{1\to2}, \epsilon_{2\to3}]$	$[\epsilon_{2\to3}, \epsilon_{3\to4}]$	$[\epsilon_{3\to4}, \epsilon_{4\to5}]$	$[\epsilon_{4\to5}, \epsilon_{5\to6}]$	$[\epsilon_{5\to6}, \epsilon_{\rm pl}]$	$[\epsilon_{\rm pl}, \pi/2]$
$\langle n_R(2)\rangle < \langle n_R(1)\rangle$	$\langle n_R(3)\rangle < \langle n_R(1)\rangle$	$\langle n_R(4)\rangle < \langle n_R(1)\rangle$	$\langle n_R(5)\rangle < \langle n_R(1)\rangle$	$\langle n_R(6)\rangle < \langle n_R(1)\rangle$	$\langle n_R(1)\rangle < \langle n_R(6)\rangle$

have

$$\tau_{\rm pl} = 1.353 + \pi k/2 \tag{16}$$

for large k, and in other words, let $\tau_{\rm pl} = \pi k/2 + \epsilon_{\rm pl}$, then $\epsilon_{\rm pl} = 1.353$. As shown in Fig. 3, r^* is plotted versus τ, and we see staircases, where r^* is increasing by unit steps, as our theory predicts, and then a sudden plunge. The staircase structure and plunges of r^* versus τ are found in the whole range of τ and are not limited to the large-τ limit studied presented analytically in Table I.

A general formalism to obtain the transition ϵ is stated as follows. We find using $F_n \ll 1$ valid from the large-τ limit and Eq. (6),

$$\langle n_R(r)\rangle \sim r \Big/ \sum_{n=1}^{r} F_n. \tag{17}$$

Then the condition for the transition τ that leads to $\langle n_R(r)\rangle = \langle n_R(r+1)\rangle$ reads

$$F_{r+1} = \sum_{n=1}^{r} F_n/r. \tag{18}$$

With $P_{\rm det}^r = \sum_{n=1}^{r} F_n$, the transcendental equation Eq. (18) becomes

$$P_{\rm det}^r(\epsilon) = rF_{r+1}(\epsilon), \tag{19}$$

which yields a set of values of τ and r, and as noted above this gives $\langle n_R(r)\rangle = \langle n_R(r+1)\rangle$. Now exploiting the fact that the values of r^* have a staircase structure, we start with $\epsilon = 0$, and then $r^* = 1$, increasing ϵ, we get the transition point $r^* = 1 \to r^* = 2$, denoted by $1 \to 2$ transition. We then continue increasing ϵ to find the transition $2 \to 3$, etc. This means that the above formula yields the values of r^* at sampling times given by ϵ. This is a valid approximation in the case of large τ only as mentioned, and in this case, with Eq. (10) we have to solve for

$$\sum_{n=1}^{r} \frac{1}{n}\cos^2\left(2n\epsilon - \frac{\pi}{4}\right) = \frac{r}{r+1}\cos^2\left[2(r+1)\epsilon - \frac{\pi}{4}\right], \tag{20}$$

and again we must increase ϵ from zero using $r = 1$, to find the first transition $r^* = 1 \to r^* = 2$ at $\epsilon_{1\to 2}$, and then update to $r = 2$ finding the transition point $\epsilon_{2\to 3}$, etc. It is clear that when r is very large, there is no solution to Eq. (20). Since the summation term in the left-hand side of Eq. (20) can be simplified as $(1/2)\sum_{n=1}^{r}[1/n + \sin(4n\epsilon)/n]$, and in the large-$r$ limit, $\sum^{r} \sin(4n\epsilon)/n \to (\pi - 4\epsilon)/2$, and $\sum^{r} 1/n \to \infty$ does not converge, while the right-hand side is always bounded by 1. Physically, it makes sense that we cannot witness the transitions forever, since as mentioned $\langle n_R(r)\rangle$ is proportional to r in the large-r limit, there must exist a minimum at finite r. We cannot expect a restart strategy to be useful for $r \gg 1$. See Fig. 4 for the comparison between exact results and approximations [Eq. (20), Table I(a)].

After finding the optimal r^*, we study the mean $\langle n_R(r^*)\rangle$, at the optimal choice r^*, which is of course the fastest way in mean sense to detect the particle. Note that when $F_n \ll 1$,

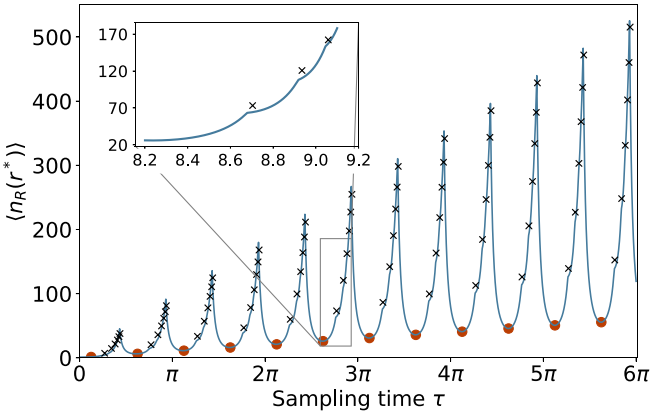

FIG. 6. The optimal mean $\langle n_R(r^*)\rangle$ vs τ for $\delta = 0$ (cyan curve). The black crosses representing $\langle n_R(r^*)\rangle$ at transition τ's are plotted using Eq. (23). And at those transitions, nonsmoothness $\langle n_R(r^*)\rangle$ is witnessed (see the inset). The minima of $\langle n_R(r^*)\rangle$ are predicted by Eq. (25) and presented by red closed circles. As shown in the figure, $\langle n_R(r^*)\rangle$ exhibits large fluctuations and periodic-like behavior when the sampling time τ is varied. The peaks of $\langle n_R(r^*)\rangle$ are found close to the plunges of r^* shown in Fig. 3, namely close to the instability points like the one presented in Fig. 5. See more details about the plot in Appendix C. For an efficient search one clearly needs to consider the optimization of the process both with respect to the restart time, but also with respect to the sampling period τ, and we will analyze this issue later.

using Eq. (17), we have

$$\langle n_R(r^*)\rangle \sim \frac{r^*}{\sum^{r^*} F_n}. \tag{21}$$

From above arguments Eq. (18), at those transition τ, we have

$$\langle n_R(r^*)\rangle \sim \frac{1}{F_{r^*+1}}. \tag{22}$$

This is obtained by calculating F_n, at the corresponding ϵ, namely, using Eq. (10),

$$\langle n_R(r^*)\rangle \sim \frac{(r^*+1)\pi\tau}{\cos^2[2(r^*+1)\tau - \pi/4]}. \tag{23}$$

See Fig. 6 for the numerical confirmation. The exact results are represented by the cyan line. And the theoretical $\langle n_R(r^*)\rangle$ at transition τ's calculated by Eq. (23) are represented by black crosses, at which nonsmoothness of $\langle n_R(r^*)\rangle$ appears. As τ is increased, the general trend is an increase of $\langle n_R(r^*)\rangle$, which is expected since the wave packet for large τ has spread out far from the detector when $\delta = 0$. In addition to this trend we have a periodical set of maxima. Note the dramatic changes in those maxima presented in the figure. The maxima are at the plunge τ's, where r^* falls from 6 to 1. The minima of $\langle n_R(r^*)\rangle$ are actually the minima of $\langle n_R(1)\rangle = 1/F_1$, when $r^* = 1$, namely

$$\min[\langle n_R(r^*)\rangle] = \min[\langle n_R(r^* = 1)\rangle]. \tag{24}$$

Later we will discuss this again. In the large-τ limit, using Eq. (10), we find when $\tau = \pi/8 + k\pi/2$, $\max(F_1) =$

$(\pi^2/8 + k\pi^2/2)^{-1}$, then the minima of $\langle n_R(r^*)\rangle$ is

$$\min[\langle n_R(r^*)\rangle] = \frac{1}{\max(F_1)} = \frac{\pi^2}{8} + k\frac{\pi^2}{2}. \tag{25}$$

We plot in closed circles these theoretical minima indicated by Eq. (25). Our theory Eqs. (23) and (25) nicely matches the numerics, as shown in Fig. 6.

B. Nearest-neighbor detection: $\delta = 1$

Here we investigate the case where the detector is put at the neighboring site to the origin, namely $\delta = 1$. In the Zeno regime, namely $\tau \to 0$, using Eq. (8), we have

$$\langle n_R(1)\rangle \sim 1 + \tau^{-2}, \quad \langle n_R(2)\rangle \sim \tfrac{5}{2} + \tau^{-2},$$
$$\langle n_R(3)\rangle \sim \tfrac{14}{3} + \tau^{-2}, \ldots. \tag{26}$$

Hence $r^* = 1$ when $\tau \to 0$. The physical picture is the following: For small τ we have a leakage of amplitude, from the starting point $x = 0$, both to $x = 1$ and to $x = -1$, in fact the amplitudes at these states are the same. Now one tries to detect on $x = 1$ and does not find the particle. One may choose to restart, which means that the amplitude at $x = -1$ restores to $x = 0$. This benefits detection. If looking at the asymptotics of the first-hitting probability, then, with Eq. (5), we find in the limit $\tau \to 0$,

$$F_1 \sim \tau^2 - \tau^4, \quad F_2 \sim \tau^2 - 5\tau^4, \quad F_3 \sim \tau^2 - 11\tau^4, \cdots. \tag{27}$$

So $F_1 > F_2 > F_3 > \cdots$, indicating that continuing with the measurement is not beneficial and a restart is the best option to speed up search. Hence performing restart after each failed measurement is the best strategy, and $r^* = 1$ when $\tau \to 0$. In the opposite limit of large τ, we have

$$F_n \sim \frac{1}{n\pi\tau}\cos^2\left(2n\tau - \frac{3\pi}{4}\right). \tag{28}$$

For $\tau = \pi k/2$, we find again that $F_n \sim (2n\pi\tau)^{-1}$, and $r^* = 1$, the same as Eqs. (11) and (12). To be more specific, since F_n is a monotonic decaying function, for these special values of τ the best strategy is to restart after the first measurement. Similarly to the case $\delta = 0$, we expect that increasing τ in every interval $[\pi k/2, \pi(k+1)/2]$ leads to the quanta jumps of r^*. While it is noteworthy that if we let $\tau = \pi k/2 - \epsilon$ with $k \gg 1$, then Eq. (28) becomes

$$F_n \sim \frac{1}{n\pi\tau}\cos^2\left(-2n\epsilon - \frac{3\pi}{4}\right) = \frac{1}{n\pi\tau}\cos^2\left(2n\epsilon - \frac{\pi}{4}\right), \tag{29}$$

which recovers to the case $\delta = 0$. This means that in the range $\tau \in [\pi k/2, \pi(k+1)/2]$, F_n in the case of $\delta = 1$ is symmetric to that in the case of $\delta = 0$, with respect to $\tau = \pi k/2 + \pi/4$, when k is large, as shown in Fig. 7. Therefore, we expect the behaviors of r^* in the case $\delta = 1$ is a mirror reflection to that in the case $\delta = 0$ in every interval $[\pi k/2, \pi(k+1)/2]$, with the symmetry axis at $\pi k/2 + \pi/4$. Then the transition ϵ's are associated via $\epsilon \leftrightarrow \pi/2 - \epsilon$ when δ switches between 0 and 1. In Fig. 8 we plot $r^*(\tau)$ with $\tau \in [0, 2\pi]$, and the staircase structure is symmetric to the previous case, even when τ is not large. In the large-τ limit, there appears definite symmetry (as seen in Fig. 9).

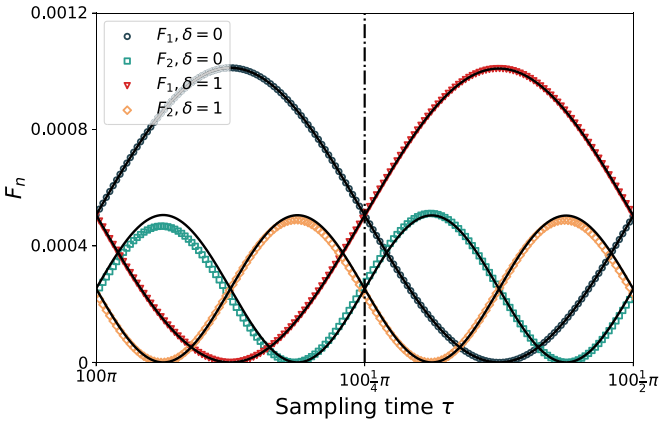

FIG. 7. F_n vs $\tau \in [100\pi, 100\frac{1}{2}\pi]$ for $n = 1, 2$ and $\delta = 0, 1$. The black curves represent the trigonometric approximations Eqs. (10) and (28). As shown and mentioned in texts, the F_n's for $\delta = 1$, in each interval $[\pi k/2, \pi(k+1)/2]$, are symmetric to the ones for $\delta = 0$ about $\pi k/2 + \pi/4$ (the dashed line).

A calculation similar to that in Table I is provided in Appendix D. And in the case $\delta = 1$ we have a sudden rise in r^*, unlike the plunge for $\delta = 0$. The rise τ, denoted by τ_r, is equal to $\pi/2 - \epsilon_{\rm pl} \approx 0.218$. And those transition ϵ are all symmetric to that in the case $\delta = 0$ about $\pi/4$, as expected. See Fig. 9 for a comparison between the exact results and approximations.

Furthermore, one can readily show that in the case of even or odd δ, Eq. (10) or Eq. (28) always hold, respectively, and the pattern presented in Fig. 9 is generic. This insightfully indicates the δ independence of F_n for all even or odd δ, in the large-sampling-time limit (similar properties are shown in Ref. [55]). In other words, large τ renders F_n's dependence only on the parity of distance between the initial and detected

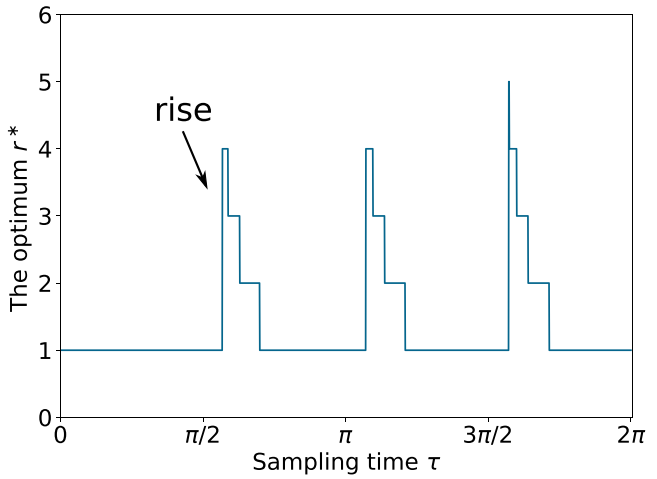

FIG. 8. The optimal restart time r^* as a function of τ for $\delta = 1$. We see the staircase structure along with periodical rises, i.e., r^* jumping from 1 to 4 or 5 (see the arrow). The series of plateaus declines from the maximum from left to right unlike the case $\delta = 0$ where we find the opposite trend (see Fig. 3).

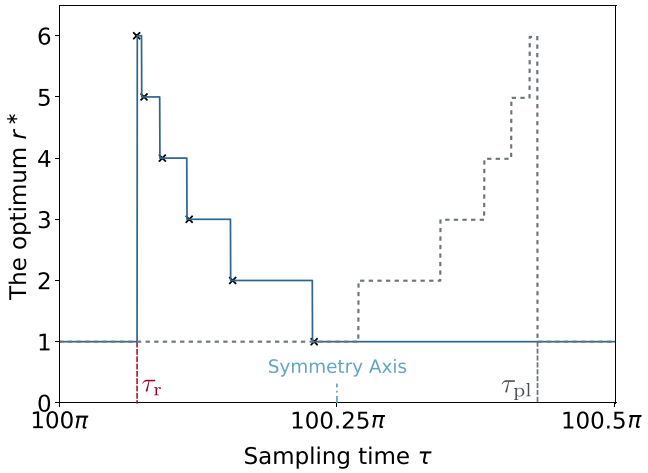

FIG. 9. r^* versus τ with $\tau \in [100\pi, 100.5\pi]$ and $\delta = 1$. The cyan lines are the exact results obtained using Eq. (6), and the black crosses represent the approximations [via applying $\epsilon \to \pi/2 - \epsilon$ to Eq. (20)]. τ_r here is approximated as $k\pi/2 + 0.218$ with $k = 200$. There is a mirror image of Fig. 4 (the gray dashed line here), so the parity of the initial condition determines the staircase structure which otherwise is universal in the sense that it does not depend on the initial condition. The symmetry axis for the two staircase patterns is $k\pi/2 + \pi/4$ with $k = 200$ here.

sites. We will see this more clearly after the discussion on $\delta = 2$.

C. Next-nearest-neighbor detection: $\delta = 2$

When $\delta = 2$, in the limit of $\tau \to 0$, we find using Eq. (5)

$$F_1 \sim \tfrac{1}{4}\tau^4 - \tfrac{1}{6}\tau^6, \quad F_2 \sim \tfrac{9}{4}\tau^4 - 6\tau^6,$$
$$F_3 \sim \tfrac{25}{4}\tau^4 - \tfrac{235}{6}\tau^6, \cdots. \tag{30}$$

Namely $F_1 < F_2 < F_3 < \cdots$ until some $n \sim 1/\tau$ and then decreases. This behavior is very different if compared with the cases $\delta = 0$ and $\delta = 1$, where F_1 was the maximum of the set $\{F_1, F_2, F_3, \ldots\}$. We expect that r^* exhibits divergence in this limit, see Fig. 10. Checking the asymptotics of $\langle n_R(r)\rangle$, with Eq. (8), we have

$$\langle n_R(1)\rangle \sim 4\tau^{-4}, \quad \langle n_R(2)\rangle \sim \tfrac{4}{5}\tau^{-4},$$
$$\langle n_R(3)\rangle \sim \tfrac{12}{35}\tau^{-4}, \cdots. \tag{31}$$

Hence $\langle n_R(1)\rangle > \langle n_R(2)\rangle > \langle n_R(3)\rangle > \cdots$. We use the theory in Ref. [48] to study the Zeno limit.

Assuming large τ, F_n is re-expressed as [54,55]

$$F_n \sim \frac{1}{n\pi\tau}\cos^2\left(2n\tau - \frac{\pi}{4}\right). \tag{32}$$

This is the same as in the case $\delta = 0$, since the initial condition δ only affects the phase in F_n via $\pi\delta/2$, and then the same parity of δ leads to the same F_n, and to the same pattern of $r^*(\tau)$. Thus we could use Table I(a) to approximate r^*'s staircase structure in this case, see Fig. 11.

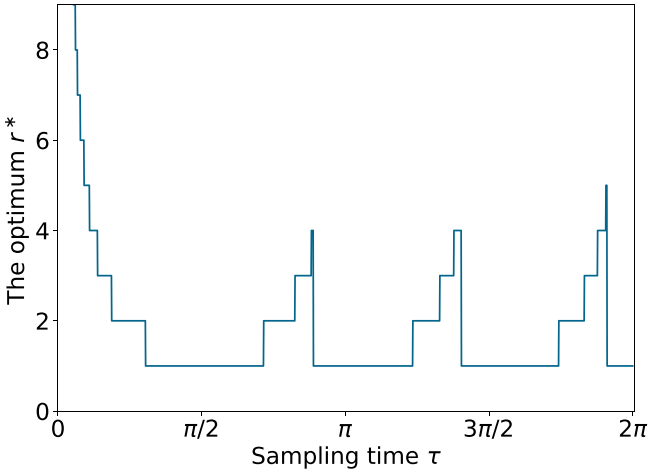

FIG. 10. The optimal restart time r^* as a function of τ for $\delta = 2$. We see the staircase structure along with periodical plunges.

D. The parity of δ matters

Following above discussion, we note a remarkable feature of the quantum first-hitting times probabilities, namely that beyond a phase, they are independent of δ:

$$\text{For even } \delta: \quad F_n \sim \frac{1}{n\pi\tau}\cos^2\left(2n\tau - \frac{\pi}{4}\right),$$
$$\text{For odd } \delta: \quad F_n \sim \frac{1}{n\pi\tau}\cos^2\left(2n\tau - \frac{3\pi}{4}\right). \tag{33}$$

This is obtained with the large argument asymptotics for $J_n(x)$, which was also used in the case of return in Ref. [54], and in the supplemental material of Ref. [55]. Equation (33) is valid in the large-τ limit, and we note that when n is large, the first-detection probability F_n transits to a n^{-3} power-law decay [54,55], but this does not affect our theory, which only focuses on finite r restart.

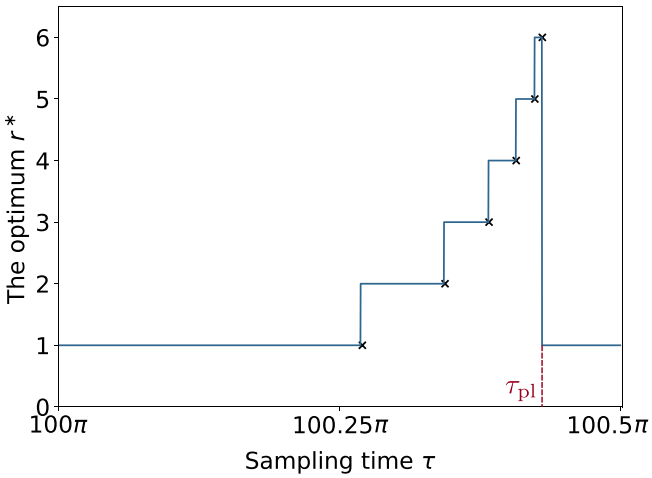

FIG. 11. r^* versus τ with $\tau \in [100\pi, 100.5\pi]$ and $\delta = 2$. The cyan lines are the exact results, and the black crosses represent the approximations using Table I(a). τ_{pl} here is approximated as $100\pi + 1.353$.

Hence, based on Eq. (33), the staircase patterns, are *binary* and merely determined by the parity of δ. These two patterns are mirror reflection to each other, connected by the operation or mapping $\epsilon_{k+1\to k} \leftrightarrow \pi/2 - \epsilon_{k\to k+1}$. The origin of universality of staircase is related to the fact that, for large τ, the first-detection amplitude is directly associated to the wave function of the measurement-free process. This then leads to specific phases in the asymptotic expansion Eq. (33) which depends on the parity only. We note that related work on discrete-time quantum walks also found interesting effects for the parity on the probability distribution of a walker's position, see Refs. [76,77].

To put it differently, a unity change of the distance between the target and source δ, in units of the lattice constant, results in a "flipping" of the staircase pattern of the optimal restart time, which again indicates, in our view, a type of instability. This effect was demonstrated in Figs. 4, 9, and 11.

V. THE ROBUSTNESS OF INSTABILITY AGAINST PERTURBATIONS IN τ

In this section, we discuss the effects of precision of the sampling time τ on the instability. In experiments, one cannot perfectly achieve the stroboscopic measurement protocol, namely there could be some random variation around the preset sampling time or measurement period τ. Hence, the practical sampling time, denoted by $\tilde{\tau}$, is fluctuating around τ. This randomness in the ideal periodicity of measurements, would have non-negligible influences, when becoming considerable. In particular such noise could possibly modify the probability F_n's oscillatory behaviors [78], and thereby probably eliminates the instability exposed in this paper. Will the instability be present when the noise is weak? And how much randomness will eliminate the instability? These issues are addressed below using numerical methods.

Without loss of generality, we chose uniformly distributed deviation from the ideal sampling time τ. Specifically, the relative deviation $|\tilde{\tau} - \tau|/\tau$ is uniformly distributed in the interval $[-w, w]$, with w chosen as 0.1, 0.2, and 0.3 in this work. Namely the actual $\tilde{\tau}$ is uniformly distributed within $[\tau(1-w), \tau(1+w)]$, and hence w characterizes the noise level affecting the precision of sampling time. Inspired by the unstable behaviors in the vicinity of the plunge τ, where we witnessed two minima competing with each other, as demonstrated in Fig. 5, we chose the ideal $\tau = 1.35$ and the return case $\delta = 0$ and observe how the noise level w affects the behaviors of those two minima.

It is noteworthy that we numerically study the issue for quantum hitting times under restart with random $\tilde{\tau}$ and Eq. (6) is invalid since the denominator $P^r_{\rm det} = \sum_{n=1}^{r} F_n$ is not constant, leading to the number of restart not obeying a geometric distribution anymore [48]. Thus, we employ the Monte Carlo method to perform simulations. The procedures are described as follows:

(i) *Initialization of the quantum walker:* The quantum walker is initially evolved from a predefined state in accordance with the Schrödinger equation. This evolution occurs over a time duration, $\tilde{\tau}_1$, which is a uniformly random variable within the range $[\tau(1-w), \tau(1+w)]$.

(ii) *Random coin tossing for detection assessment:* A random variable, referred to as a "coin," is generated. This variable is uniformly distributed within the interval [0, 1]. The purpose of the coin is to ascertain whether the quantum walker is detected following the initial state's evolution. This determination is made by comparing the coin's value with the detection probability, which is derived from the unitary evolution.

(iii) *Non-detection and state modification:* If the coin value falls below the computed detection probability, then we are done and the hitting time is 1. If the coin value exceeds the computed detection probability, then it signifies that the walker remains undetected. In this case, the amplitude at the target site $|0\rangle$ is erased, and the wave vector is renormalized. Subsequently, the single-site-erased wave vector undergoes unitary evolution for a duration, $\tilde{\tau}_2$. Notably, $\tilde{\tau}_2$ is an independent and identically distributed random value, akin to $\tilde{\tau}_1$. The objective is to compute the probability of detection at the time $t = \tilde{\tau}_1 + \tilde{\tau}_2$.

(iv) *Repeated detection attempts:* Post the initial nondetection, a second independent and identically distributed coin is generated and compared with the newly computed detection probability to decide if the walker is detected at this stage, as in the step (iii).

(v) *Criteria for repetition termination under sharp restart:* The process iterates until the coin value is less than the computed probability of detection, marking the end of a repetition cycle. Alternatively, if the process extends up to a preset fixed restart step r (i.e., after a cumulative time of $t = \tilde{\tau}_1 + \tilde{\tau}_2 + \cdots + \tilde{\tau}_r$) and the walker remains undetected, the entire procedure recommences from the initial state, repeating the procedures (i)–(v).

(vi) *Restarted hitting time calculation:* Once we get, for the first time, the scenario where the coin value falls below the computed probability of detection at the corresponding time, the process is done. The number of all preceding unsuccessful attempts, incremented by 1, is recorded as the first-detection time, or the hitting time, under the restart condition [79].

(vii) *Realizations and expected value determination:* The aforementioned procedures, executed for obtaining a single value of the hitting time n_R under r-step restarts, is called a single realization. To ascertain the expected value of n_R as a function of r, large number of realizations are conducted for each value of r.

This was implemented with a *Python* program, generating the results presented in Fig. 12, for three different levels of noise w, i.e., 0.1, 0.2, 0.3. We note that, since computers cannot simulate the dynamics of an infinite line, practically, a line of 120 sites was used to approximate the unbounded model, and the maximal restart step is chosen as 15 to ensure that the boundary does not affect the dynamics of the wave packet prior to restart (i.e., $15\tau(1+0.3)\cdot\max(v_g) = 15 \times 1.35 \times 1.3 \times 2 = 52.7 < 120/2$, where as mentioned the group velocity $v_g = \partial_k E(k)$, and the initial site is set in the middle of the line). As seen, the instability is robust, in the sense that the presence of two minima is clearly visible for $w = 0.1$ and $w = 0.2$, indicating that the basic phenomenon is immune to noise. For $w = 0.3$ the existence of a pair of minima is somewhat vague, and hence roughly when $w = 0.3$, the effect we have found in the main text is wiped out.

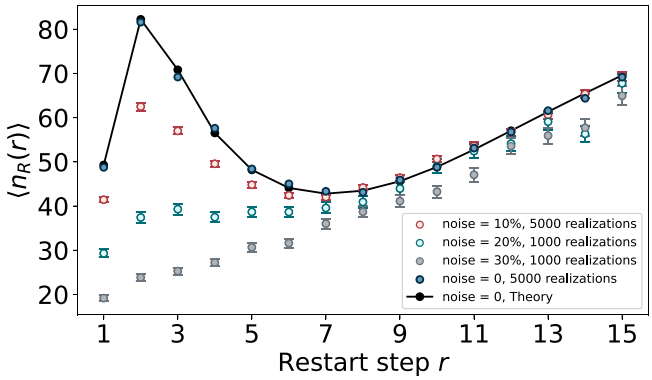

FIG. 12. The mean hitting time under restart $\langle n_R(r)\rangle$ versus restart step r for different levels of noise characterized by the width of the distribution of $\tilde{\tau}$. We see the appearance of two minima of $\langle n_R(r)\rangle$ when the noise is chosen as 0.1, 0.2 fluctuating around $\tau = 1.35$, while the absence of two minima when the noise is 0.3. Hence the instability is quite robust under noise in the sampling time. The zero-noise data are for confirmation of the validity of the theory Eq. (6). The simulations are obtained using Monte Carlo methods as described in the text.

VI. OPTIMIZATION WITH RESPECT TO BOTH τ AND r

In this section we will not deal with the noise problem. All the above discussions focus on the optimal restart time for given sampling time τ, and a natural question arises from the existence of a globally optimal choice (τ^*, r^*) that achieves a global optimization of the mean $\langle n_R\rangle$, with regard to both controlling parameters. We note here that the number of measurements until the first-detection is minimized in this work, and the global optimization of the expected time is left for future study.

The function $\langle n_R(r^*)\rangle$ has multiple minima, as shown already in Fig. 6. We also present $\langle n_R(r^*)\rangle$ for cases $\delta = 1$ and $\delta = 2$ in Fig. 13. As mentioned in Eq. (24) and likewise here, in the large-τ limit which validates the $J_\alpha(x)$ approximated as trigonometric functions, using Eq. (33), all the minima of $\langle n_R(r^*)\rangle$ are found at $\tau = \tau^\dagger$ minimizing $\langle n_R(r^* = 1)\rangle$, i.e.,

$$\min[\langle n_R(r^*)\rangle] = \pi\tau^\dagger, \quad \text{with}$$
$$\tau^\dagger = (-1)^\delta \pi/8 + k\pi/2, \quad \text{and} \quad r^* = 1. \tag{34}$$

Here k is a large integer. Eq. (34) is valid for large k or τ. It is not surprising that in this large-τ limit $r^* = 1$, since the wave packet has a long time to evolve, and hence statistically the particle is far from the target after and before the first measurement, thus it is wise to restart. Unfortunately, or not, the global minimum as found, for example in Fig. 13, is found for small τ, provided that δ is also small. For large δ, as we discuss below, special features emerge.

We conjecture, that even beyond the large-τ limit, the global minimum is found for $r^* = 1$. More specifically, let r^*, τ^* be the sampling time and restart time that minimize $\langle n_R\rangle$, and we suggest:

$$\langle n_R(r^*, \tau^*)\rangle = \frac{1}{F_1(\tau^*)} = \frac{1}{\max(F_1)}. \tag{35}$$

Recall that $F_1 = J_\delta^2(2\tau)$ [see Eq. (5)], and thus $r^* = 1$ and $\tau^* = \xi_\delta/2$, where $t = \xi_\alpha$ marks the highest peak of $J_\alpha(t)$, give the global minimum of $\langle n_R\rangle$. Equation (35) should hold for any value of δ. Nevertheless, an estimate for τ^*, which becomes more accurate for large δ, can be found in the recently published literature. References [80,81] show that $2\tau^* = \xi_\delta \sim \delta$, whose numerical confirmation, as well as exact numerical solutions for other extrema of $J_\alpha(t)$ (also used in Fig. 13, the data presented by crosses), can be found in the supplementary material of Ref. [80]. Thus, the global minimum is given by

$$r^* = 1, \quad \tau^* \sim \frac{\delta}{2} = \frac{\delta}{\max(v_g)} =: t_{\rm inc}, \tag{36}$$

where $t_{\rm inc} = \delta/2$ is the incidence time (in time units with $\gamma = 1$) during which the wave front travels from $|0\rangle$ to $|\delta\rangle$ (see Fig. 1). Hence, as mentioned, this suggests that $\tau^* \simeq \delta/2$ becomes a better approximation as δ grows, namely for large δ, $t_{\rm inc}$ gives a good estimate of the globally optimized sampling time τ^*. This again manifests the ballistic spreading of the wave packet's wave front. See Fig. 14, where we witness that

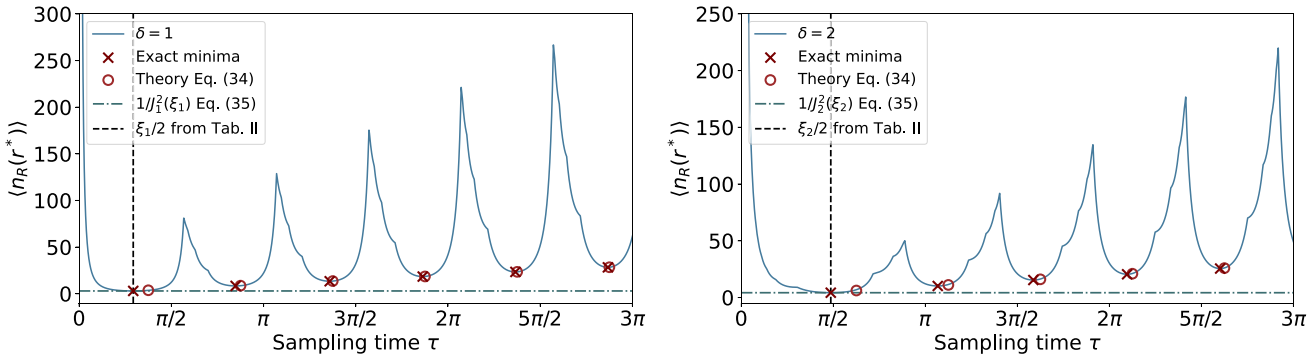

FIG. 13. The optimal mean $\langle n_R(r^*)\rangle$ vs τ for $\delta = 1$ (left) and $\delta = 2$ (right). The numerically obtained exact minima (crosses) converge to the theoretical results (open circles) calculated with Eq. (34) as τ becomes larger. We see that the global optimization (leftmost cross) with respect to both τ and r is achieved for $\tau = \xi_\delta/2$ (vertical dashed lines, obtained from Eq. (35) and Table II) that minimizes $\langle n_R(1)\rangle = [J_\delta(2\tau)]^{-2}$ (horizontal dashdotted lines), i.e., when $F_1(\tau) = J_\delta^2(2\tau)$ reaches its global maximum. The result clearly shows that Eq. (35) is an excellent approximation.

TABLE II. The numerical τ^* minimizing $\langle n_R\rangle$, the maximum of $J_\delta^2(2\tau)$, $\xi_\delta/2$, and the incidence time $t_{\rm inc}=\delta/2$, for different δ. Recall that in our system the maximal group velocity is 2, hence $\delta/2$ is the incident time, for a particle initially at a distance δ from the detector.

δ	1	2	3	6	9	12	20	40	100
$t_{\rm inc}$	0.500	1.000	1.500	3.000	4.500	6.000	10.000	20.000	50.000
$\xi_\delta/2$	0.921	1.527	2.101	3.751	5.356	6.940	11.110	21.393	51.884
τ^*	0.920	1.527	2.100	3.751	5.356	6.940	11.109	21.394	51.883

Eq. (36) also works well for not-too-large δ, i.e., $\delta=9$, 12. As expected, for $\delta=100$, presented in Fig. 15, the approximation works even better, see also Table II. The global optimum is physically interpretable, since this special τ allows the largest part of the wave packet to arrive at the target state, once collapsed, it is best to start anew, namely a restart. For small δ, say, 1,2, Eq. (35) is tested in Fig. 13. For this test we find the maximum of $|J_\delta(2\tau)|$ semianalytically with a simple program. We see that Eq. (35) is valid for small δ, and while it holds also for large δ, Eq. (36) is simpler. We will now analyze the reliability of our conjecture Eq. (35), where the key is whether the global minimum always occurs for $r=1$.

When δ is large, namely it takes a long time to reach the target, we expect that large τ is useful. We can prove that in the large-τ limit, the minima of $\langle n_R(r^*)\rangle$ is always when $r^*=1$. To do this, one needs to justify that the minima of $\langle n_R(1)\rangle$ are smaller than those of $\langle n_R(r)\rangle$ for any $r\geqslant 2$ in every interval of resemblance. Recall that for large τ, the mean detection time exhibits periodic-like behaviors, see Fig. 6, and hence we have intervals or resemblance. With Eq. (8), the equivalent statement is that the maximum of $J_\delta^2(2\tau)$ is larger than that of $1/\langle n_R(r)\rangle$ for any $r\geqslant 2$, hence in the large-τ limit approximation,

$$\max\left[\frac{1}{\langle n_R(1)\rangle}\right]=\max\left[J_\delta^2(2\tau)\right]>\max\left[\frac{\sum_{n=1}^r F_n(\tau)}{r}\right]_{r\geqslant 2}. \tag{37}$$

Namely, this simply states that the maximum of $J_\delta^2(2\tau)$ exceeds that of the average of all the F_n until $n=r$, and clearly $\sum_{n=1}^r F_n(\tau)/r\leqslant \max[F_n(\tau)]$. This can be proven by illustrating that the maximum of $J_\delta^2(2\tau)$ is larger than the maximum of any F_n when $n>1$. Using the large-x approximation of $J_\nu(x)$, it is just to show that the maxima of $(1/\pi\tau)\cos^2(2\tau-\pi\delta/2-\pi/4)$ are larger than the maxima of $(1/n\pi\tau)\cos^2(2n\tau-\pi\delta/2-\pi/4)$, with the integer $n\geqslant 2$. This is obvious since the latter is enveloped by $1/n\pi\tau$. Hence in the large-τ limit, we can readily verify Eq. (37) and prove that the minima of $\langle n_R(r^*)\rangle$ occur at $r^*=1$. Further, the envelope of F_1, $1/\pi\tau$, indicates that the minima of $\langle n_R(r^*)\rangle$ are also growing with τ, as seen in Eq. (34) and Fig. 13. See also Fig. 15 for the numerical confirmation and the incidence time $t_{\rm inc}$ as a good approximation for τ^* when δ is large.

Although it is difficult to rigorously prove the dominance of $r^*=1$ in attaining the global minimum of $\langle n_R(r^*)\rangle$, for any value of δ, it is physically reasonable and interpretable. The interpretation is that the wave packet's wave front propagates ballistically, as quantified by the Bessel function $J_\delta^2(2t)$, rendering the detection probability reaching its maximum when the detector captures the wave front (see Fig. 1). Since the detector in our setup is fixed at the target site and switched on-off stroboscopically, if we choose the first "on" time, at $t=\tau$, coinciding with the juncture wherein the wave packet's wave front encompasses the target site, this temporal alignment will maximize the probability of particle detection. In the event of detection failure, recommencing the experimental process is advantageous, as it offers the highest likelihood of subsequent successful particle detection. In this sense, the global optimization requires the specific τ^* that maximizes $J_\delta^2(2\tau)$ and thus minimizes $\langle n_R(1)\rangle$, indicating $(1,\xi_\delta/2)$ as the

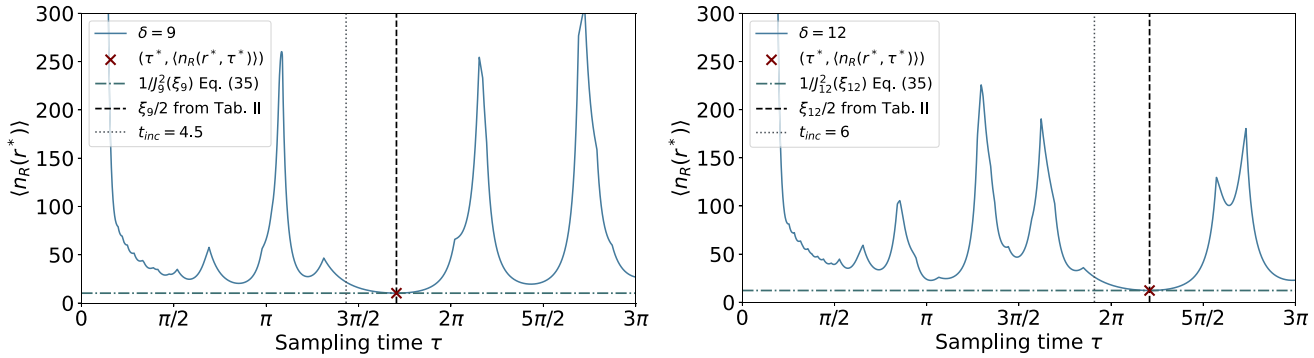

FIG. 14. The optimal mean $\langle n_R(r^*)\rangle$ vs τ for $\delta=9$ (left) and $\delta=12$ (right). We see that the numerical global minimum of $\langle n_R(r^*)\rangle$ (crosses) is matched by our theory Eq. (35), namely $\langle n_R(1,\xi_\delta/2)\rangle=[J_\delta(\xi_\delta)]^{-2}$ (see the vertical dashed lines and horizontal dashdotted lines, obtained from Table II). The incidence time $t_{\rm inc}=\delta/2$ (vertical dotted lines) also provides a rough approximation for τ^*. Thus, we conjecture that the most efficient detection strategy, in the sense of the least number of measurement attempts, is to restart after the first measurement with the largest success probability in the first measurement.

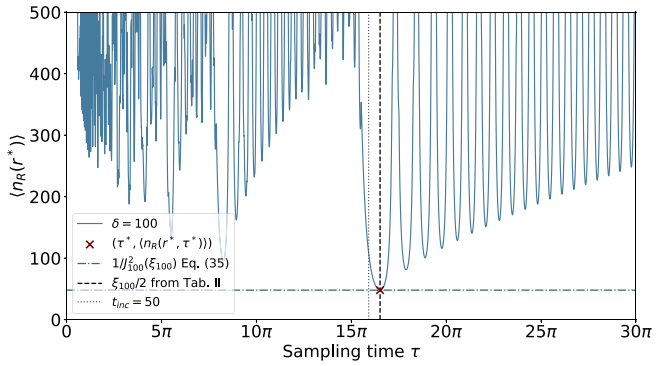

FIG. 15. The optimal mean $\langle n_R(r^*)\rangle$ vs τ for $\delta = 100$. We see that the exact global minimum of $\langle n_R(r^*)\rangle$ (cross) is matched by the minimum of $\langle n_R(1)\rangle = [J_{100}(2\tau)]^{-2}$ (the horizontal line) at $\tau = \xi_{100}/2$ (the vertical dashed line, see Table II), and the incidence time $t_{\rm inc} = \delta/2$ (vertical dotted line) gives pretty good approximation for τ^*.

optimal set of parameters. Notably, in large-δ cases, a good approximation is $\tau^* = \xi_\delta/2 \simeq \delta/2$ (Fig. 15).

VII. SUMMARY

With restarts introduced to quantum hitting times, we find features that expose the instability existing in the optimization of the mean hitting time. The first feature is the presence of *several minima* of the mean hitting time [48] rather than one unique minima, as in the classical case [1]. This is due to the interference-induced quantum oscillations, indicated by the Bessel function $J_n(x)$ in Eq. (2) and the graphic illustration in Fig. 1. These oscillations are found features of the solution to the Schrödinger equation, and the quantum first-hitting time probability F_n in the absence of restarts. These are general aspects of quantum dynamics, so we expect that our results will have a wider application than the model presented here.

Then the challenge is to find the optimum of the mean hitting time under restart. For large τ (in units $\gamma = 1$), we showed that $r^*(\tau)$ possesses a staircase structure of period $\pi/2$, accompanied by plunges or rises, see Figs. 4, 9, and 11. We note that the r^* here is the optimal choice of the restart step r for a given sampling time τ. Furthermore, there are two symmetric patterns of staircases, determined by the *parity* of the distance between the initial and detected sites (in units of the lattice constant). All those findings depict the instability existing in the quantum restart problems. Namely, slight changes of τ lead to a large change of $\langle n_R(r)\rangle$ (Fig. 2), optimum switching between different minima (Fig. 5), and change of the parity of δ causes a "flipping" of the staircase pattern of the optimal restart time. We want to note that the instability is not limited in the large-τ case, and it is also found for small τ though then the staircases do not converge to an asymptotic limit, see the small-τ limit of Fig. 3. Since the instability is essentially attributed to the oscillatory nature of the hitting time statistics, we expect its generality when changing other control parameters.

Is the instability we found in quantum restarts "robust" in the presence of external "disturbance," such as imperfect projective measurements, or nonstroboscopic measurements? We numerically study the latter with Monte Carlo simulations, through introducing uniformly distributed noise or deviations to the chosen fixed sampling time. The results indicate that the instability is quite robust when confronting the noise in sampling, in the sense that the mean hitting time around the plunge τ (in Fig. 5), still exhibits two minima up to a noise level of 20%, as shown in Fig. 12. Further research on the impact of different types of noise, including analytical study, is deemed worthwhile.

Another issue is the global minimum of $\langle n_R\rangle$ given a specific choice of both controlling parameters, (r^*, τ^*). We conjecture that the global optimization occurs when τ is tuned to minimize the $\langle n_R(1)\rangle$, and hence the restarts must be made after the first measurement. Roughly speaking, when the sampling time or measurement period τ is around $\tau^* = \xi_\delta/2$, which maximizes $J^2_\delta(2\tau)$, the first-detection attempt at $|\delta\rangle$ will succeed with a relatively large probability. This leads to the optimal choice of restart time at $r = 1$. In the cases where the distance between the target and initial sites is large, i.e., $\delta \gg 1$, $\xi_\delta/2$ is approximately the incidence time $t_{\rm inc} = \delta/2$, showing the ballisticity of the wave-front spreading. Hence in the sense of detecting the quantum walker with least attempts (through the sharp-restart strategy), when δ is large, restarting after the first measurement with the highest likelihood of success, performed at $\tau^* \simeq \delta/2$, is the most efficient choice. We emphasize again that we optimized here $\langle n_R\rangle$ and not $\langle n_R\rangle\tau$, so clearly more work is needed.

Can we foresee quantum experiments checking the validity of this work? A good platform for that aim are quantum computers, on which on-demand qubit resets have been achieved with the initial purpose of optimizing quantum circuits. The quantum walk dynamics can be mapped to a spin model through the Jordan-Wigner transformation [82], or other methods [46], with repeated measurements implemented by the built-in single-qubit measurements [45]. Similar experiments on finite systems, with restarts taking place after 20 measurements, have been successfully implemented [49]. This greatly enhances our confidence in verifying the theory presented in this paper for the optimization problem, though finite-size effects might be important.

In this work we considered a quantum walk on the line; however this is not an essential ingredient of our results, in the sense that quantum instabilities for the restart problem can be found also for finite systems. We also note that possibly other oscillatory dynamics or reset strategies [83], beyond the quantum case, will exhibit similar features to what we have found here. A key point to study the quantum instabilities is the use of sharp restart, which as mentioned is the optimal choice. In our previous work [48], we studied briefly quantum restarts with Poisson restarts, which did not exhibit the multiple minima found here.

ACKNOWLEDGMENTS

The support of Israel Science Foundation's Grant No. 1614/21 is acknowledged.

APPENDIX A: UNDER RESTART: THE FIRST-HITTING PROBABILITY, GUARANTEED DETECTION

1. The probability

In probability theory language, the first-hitting probability $F_n = \Pr(\overline{\mathcal{E}_1}\overline{\mathcal{E}_2}\cdots\overline{\mathcal{E}_{n-1}}\mathcal{E}_n)$, where $\mathcal{E}_k$ denotes the event of successful detection at the kth attempt, and $\overline{\mathcal{E}_k}$ means the event of failing to detect the walker at the kth attempt. Now with the deterministic restart strategy incorporated, the measurement protocol is as follows: After the rth attempt, if the walker is not yet detected, then we start anew with the same initial state, until the first successful detection at the n_Rth attempt with $n_R = r\mathcal{R} + \tilde{n}$, where $\mathcal{R}$ is the number of restart event and $\tilde{n}$ is the number of attempts until success following the last restart, and then $1 \leqslant \tilde{n} \leqslant r$, $\mathcal{R} \geqslant 0$ since the restart is made just after a measurement. Following standard statistical methods, the first-hitting probability under restart is

$$\begin{aligned} F_{n_R} &= \Pr(\underbrace{\overline{\mathcal{E}_1}\cdots\overline{\mathcal{E}_r}\overline{\mathcal{E}_1}\cdots\overline{\mathcal{E}_r}}_{\text{repeat }\mathcal{R}\text{ times}}\overline{\mathcal{E}_1}\cdots\mathcal{E}_{\tilde{n}}) \\ &= (1 - F_1 - \cdots - F_r)^{\mathcal{R}} F_{\tilde{n}} \\ &= \left(1 - \sum_{k=1}^{r} F_k\right)^{\mathcal{R}} F_{\tilde{n}}, \end{aligned} \tag{A1}$$

where F_j are the probabilities of the first-hitting at the jth attempt in the absence of restart. The last expression in Eq. (A1) is also intuitive: The term inside the brace suggests the survival probability after rth measurement, the power is the number of reset event, and the term outside the brace gives the probability of first success after the last restart, and thus the product of the two probability is F_{n_R}. Note here $\tilde{n}$ ranges from 1 to r (different from the remainder ranging from 0 to $r-1$), and $\mathcal{R} \geqslant 0$. If $r = 10$, then $F_{n_R=30}$ is $(1 - \sum_{k=1}^{10} F_k)^2 F_{10}$.

2. Proof for the guaranteed detection

The restarted total detection probability P_{det} is

$$\begin{aligned} P_{\text{det}} &= \sum_{n_R=1}^{\infty} F_{n_R} = \sum_{r\mathcal{R}+\tilde{n}=1}^{\infty} \left(1 - \sum_{j=1}^{r} F_j\right)^{\mathcal{R}} F_{\tilde{n}} \\ &= \sum_{\mathcal{R}=0}^{\infty}\sum_{\tilde{n}=1}^{r} \left(1 - \sum_{j=1}^{r} F_j\right)^{\mathcal{R}} F_{\tilde{n}} \\ &= \sum_{\tilde{n}=1}^{r} F_{\tilde{n}} \sum_{\mathcal{R}=0}^{\infty} \left(1 - \sum_{j=1}^{r} F_j\right)^{\mathcal{R}} \\ &= \sum_{\tilde{n}=1}^{r} F_{\tilde{n}} \left(\sum_{j=1}^{r} F_j\right)^{-1} = 1. \end{aligned} \tag{A2}$$

Hence the total detection probability is one provided that $\sum_{j=1}^{r} F_j \neq 0$, meaning that the particle will be eventually detected, as long as there exist finite probability of detection during one restart period.

APPENDIX B: DERIVATION FOR EQ. (6) IN THE MAIN TEXT

Here we provide an alternative derivation for the mean of n_R under restart. With Eq. (A1) and the definition $\langle n_R(r)\rangle = \sum_{n_R=1}^{\infty} n_R F_{n_R}$, we obtain

$$\begin{aligned} \langle n_R(r)\rangle &= \sum_{n_R=1}^{\infty} n_R \left(1 - \sum_{k=1}^{r} F_k\right)^{\mathcal{R}} F_{\tilde{n}} \\ &= \sum_{r\mathcal{R}+\tilde{n}=1}^{\infty} (r\mathcal{R} + \tilde{n}) \left(1 - \sum_{k=1}^{r} F_k\right)^{\mathcal{R}} F_{\tilde{n}} \\ &= \sum_{\mathcal{R}=0}^{\infty}\sum_{\tilde{n}=1}^{r} r\mathcal{R} \left(1 - \sum_{k=1}^{r} F_k\right)^{\mathcal{R}} F_{\tilde{n}} \\ &\quad + \sum_{\mathcal{R}=0}^{\infty}\sum_{\tilde{n}=1}^{r} \tilde{n} \left(1 - \sum_{k=1}^{r} F_k\right)^{\mathcal{R}} F_{\tilde{n}} \\ &= r \sum_{\tilde{n}=1}^{r} F_{\tilde{n}} \sum_{\mathcal{R}=0}^{\infty} \mathcal{R} \left(1 - \sum_{k=1}^{r} F_k\right)^{\mathcal{R}} \\ &\quad + \sum_{\tilde{n}=1}^{r} \tilde{n} F_{\tilde{n}} \sum_{\mathcal{R}=0}^{\infty} \left(1 - \sum_{k=1}^{r} F_k\right)^{\mathcal{R}} \\ &= \frac{r\left(1 - \sum_{j=1}^{r} F_j\right)}{\sum_{j=1}^{r} F_j} + \underbrace{\sum_{k=1}^{r} k F_k \left(\sum_{k=1}^{r} F_k\right)^{-1}}_{\langle n\rangle_{\text{cond}}^{r}} \\ &= r\frac{1 - P_{\text{det}}^{r}}{P_{\text{det}}^{r}} + \langle n\rangle_{\text{cond}}^{r}. \end{aligned} \tag{B1}$$

This gives the Eq. (6) in the main text.

APPENDIX C: DETAILS IN PLOTTING FIG. 6

Since Eq. (23) is valid at the transition τ, we chose $\tau = 1.369 + \pi k/2$ for $r^* = 6$ with k an integer [using Eq. (20)]. Although $r^* = 6$ is cutoff by $\epsilon_{\text{pl}} = 1.353$, we use the fact that $\langle n_R(6)\rangle(\tau = 1.353) \approx \langle n_R(6)\rangle(\tau = 1.369) = 1/F_7(\tau = 1.369)$, see Fig. 5. The black crosses nicely capture the $\langle n_R(r^*)\rangle$ at the transition τ's.

APPENDIX D: TRANSITION τ IN THE CASE OF $\delta = 1$ AND THE LARGE-τ LIMIT

$$\begin{aligned} \epsilon &\in [0, 0.218] : \langle n_R(1)\rangle = \min(\langle n_R(r)\rangle), \\ \epsilon &\in [0.218, \epsilon_{6\to5}] : \langle n_R(6)\rangle < \langle n_R(1)\rangle, \\ \epsilon_{6\to5} &= 0.239 = \pi/2 - 1.332, \\ \epsilon &\in [\epsilon_{6\to5}, \epsilon_{5\to4}] : \langle n_R(5)\rangle < \langle n_R(1)\rangle, \\ \epsilon_{5\to4} &= 0.291 = \pi/2 - 1.280, \\ \epsilon &\in [\epsilon_{5\to4}, \epsilon_{4\to3}] : \langle n_R(4)\rangle < \langle n_R(1)\rangle, \\ \epsilon_{4\to3} &= 0.367 = \pi/2 - 1.204, \end{aligned}$$

$$\epsilon \in [\epsilon_{4\to3}, \epsilon_{3\to2}] : \langle n_R(3)\rangle < \langle n_R(1)\rangle, \qquad \epsilon \in [\epsilon_{3\to2}, \epsilon_{2\to1}] : \langle n_R(2)\rangle < \langle n_R(1)\rangle,$$
$$\epsilon_{3\to2} = 0.490 = \pi/2 - 1.081, \qquad \epsilon_{2\to1} = 0.721 = \pi/2 - 0.850. \tag{D1}$$

[1] S. Gupta and A. M. Jayannavar, Front. Phys. **10**, 789097 (2022).
[2] M. R. Evans, S. N. Majumdar, and G. Schehr, J. Phys. A: Math. Theor. **53**, 193001 (2020).
[3] M. Luby, A. Sinclair, and D. Zuckerman, *Proceedings of the 2nd Israel Symposium on Theory and Computing Systems* (IEEE, Natanya, Israel, 1993), p. 128.
[4] M. R. Evans and S. N. Majumdar, Phys. Rev. Lett. **106**, 160601 (2011).
[5] D. Boyer and C. Solis-Salas, Phys. Rev. Lett. **112**, 240601 (2014).
[6] S. Gupta, S. N. Majumdar, and G. Schehr, Phys. Rev. Lett. **112**, 220601 (2014).
[7] A. Pal, A. Kundu, and M. R. Evans, J. Phys. A: Math. Theor. **49**, 225001 (2016).
[8] S. Eule and J. J. Metzger, New J. Phys. **18**, 033006 (2016).
[9] S. Reuveni, Phys. Rev. Lett. **116**, 170601 (2016).
[10] A. Pal and S. Reuveni, Phys. Rev. Lett. **118**, 030603 (2017).
[11] A. Falcón-Cortés, D. Boyer, L. Giuggioli, and S. N. Majumdar, Phys. Rev. Lett. **119**, 140603 (2017).
[12] S. Belan, Phys. Rev. Lett. **120**, 080601 (2018).
[13] A. Chechkin and I. M. Sokolov, Phys. Rev. Lett. **121**, 050601 (2018).
[14] M. R. Evans and S. N. Majumdar, J. Phys. A: Math. Theor. **51**, 475003 (2018).
[15] D. Boyer, A. Falcón-Cortés, L. Giuggioli, and S. N. Majumdar, J. Stat. Mech. (2019) 053204.
[16] A. S. Bodrova, A. V. Chechkin, and I. M. Sokolov, Phys. Rev. E **100**, 012119 (2019).
[17] L. Kuśmierz and E. Gudowska-Nowak, Phys. Rev. E **99**, 052116 (2019).
[18] B. Besga, A. Bovon, A. Petrosyan, S. N. Majumdar, and S. Ciliberto, Phys. Rev. Res. **2**, 032029(R) (2020).
[19] M. Magoni, S. N. Majumdar, and G. Schehr, Phys. Rev. Res. **2**, 033182 (2020).
[20] B. De Bruyne, J. Randon-Furling, and S. Redner, Phys. Rev. Lett. **125**, 050602 (2020).
[21] O. Tal-Friedman, A. Pal, A. Sekhon, S. Reuveni, and Y. Roichman, J. Phys. Chem. Lett. **11**, 7350 (2020).
[22] P. C. Bressloff, Proc. R. Soc. A **476**, 20200475 (2020).
[23] V. Méndez, A. Masó-Puigdellosas, T. Sandev, and D. Campos, Phys. Rev. E **103**, 022103 (2021).
[24] S. N. Majumdar, F. Mori, H. Schawe, and G. Schehr, Phys. Rev. E **103**, 022135 (2021).
[25] M. Dahlenburg, A. V. Chechkin, R. Schumer, and R. Metzler, Phys. Rev. E **103**, 052123 (2021).
[26] R. K. Singh, T. Sandev, A. Iomin, and R. Metzler, J. Phys. A Math. Theor. **54**, 404006 (2021).
[27] I. Eliazar and S. Reuveni, J. Phys. A: Math. Theor. **54**, 125001 (2021).
[28] O. Blumer, S. Reuveni, and B. Hirshberg, J. Phys. Chem. Lett. **13**, 11230 (2022).
[29] S. Ahmad, K. Rijal, and D. Das, Phys. Rev. E **105**, 044134 (2022).
[30] S. Ray, Phys. Rev. E **106**, 034133 (2022).
[31] I. I. Eliazar and S. Reuveni, J. Phys. A: Math. Theor. **56**, 024003 (2023).
[32] E. Barkai, R. Flaquer-Galmés, and V. Méndez, Phys. Rev. E **108**, 064102 (2023).
[33] B. Mukherjee, K. Sengupta, and S. N. Majumdar, Phys. Rev. B **98**, 104309 (2018).
[34] D. C. Rose, H. Touchette, I. Lesanovsky, and J. P. Garrahan, Phys. Rev. E **98**, 022129 (2018).
[35] S. Belan and V. Parfenyev, New J. Phys. **22**, 073065 (2020).
[36] A. Riera-Campeny, J. Ollé, and A. Masó-Puigdellosas, arXiv:2011.04403.
[37] G. Perfetto, F. Carollo, M. Magoni, and I. Lesanovsky, Phys. Rev. B **104**, L180302 (2021).
[38] G. Perfetto, F. Carollo, and I. Lesanovsky, SciPost Phys. **13**, 079 (2022).
[39] X. Turkeshi, M. Dalmonte, R. Fazio, and M. Schirò, Phys. Rev. B **105**, L241114 (2022).
[40] G. Haack and A. Joye, J. Stat. Phys. **183**, 17 (2021).
[41] M. Magoni, F. Carollo, G. Perfetto, and I. Lesanovsky, Phys. Rev. A **106**, 052210 (2022).
[42] S. Dattagupta, D. Das, and S. Gupta, J. Stat. Mech. (2022) 103210.
[43] F. J. Sevilla and A. Valdés-Hernández, J. Phys. A: Math. Theor. **56**, 034001 (2023).
[44] A. Acharya and S. Gupta, Phys. Rev. E **108**, 064125 (2023).
[45] S. Tornow and K. Ziegler, Phys. Rev. Res. **5**, 033089 (2023).
[46] Q. Wang, S. Ren, R. Yin, K. Ziegler, E. Barkai, and S. Tornow, arXiv:2402.15843.
[47] S. Redner, *A Guide to First-Passage Processes* (Cambridge University Press, Cambridge, UK, 2001).
[48] R. Yin and E. Barkai, Phys. Rev. Lett. **130**, 050802 (2023).
[49] R. Yin, Q. Wang, S. Tornow, and E. Barkai, arXiv:2401.01307.
[50] H. Krovi and T. A. Brun, Phys. Rev. A **74**, 042334 (2006).
[51] F. A. Grünbaum, L. Velázquez, A. H. Werner, and R. F. Werner, Commun. Math. Phys. **320**, 543 (2013).
[52] S. Dhar, S. Dasgupta, A. Dhar, and D. Sen, Phys. Rev. A **91**, 062115 (2015).
[53] S. Dhar, S. Dasgupta, and A. Dhar, J. Phys. A: Math. Theor. **48**, 115304 (2015).
[54] H. Friedman, D. A. Kessler, and E. Barkai, Phys. Rev. E **95**, 032141 (2017).
[55] F. Thiel, E. Barkai, and D. A. Kessler, Phys. Rev. Lett. **120**, 040502 (2018).
[56] F. Thiel, D. A. Kessler, and E. Barkai, Phys. Rev. A **97**, 062105 (2018).
[57] R. Yin, K. Ziegler, F. Thiel, and E. Barkai, Phys. Rev. Res. **1**, 033086 (2019).
[58] Q. Liu, R. Yin, K. Ziegler, and E. Barkai, Phys. Rev. Res. **2**, 033113 (2020).
[59] E. Farhi and S. Gutmann, Phys. Rev. A **58**, 915 (1998).
[60] O. Mülken and A. Blumen, Phys. Rep. **502**, 37 (2011).

[61] M. Grover and R. Silbey, J. Chem. Phys. **54**, 4843 (1971).
[62] N. Konno, Phys. Rev. E **72**, 026113 (2005).
[63] Y. Lahini, A. Avidan, F. Pozzi, M. Sorel, R. Morandotti, D. N. Christodoulides, and Y. Silberberg, Phys. Rev. Lett. **100**, 013906 (2008).
[64] S. Hoyer, M. Sarovar, and K. B. Whaley, New J. Phys. **12**, 065041 (2010).
[65] J. Muga and C. Leavens, Phys. Rep. **338**, 353 (2000).
[66] F. Thiel, I. Mualem, D. A. Kessler, and E. Barkai, Phys. Rev. Res. **2**, 023392 (2020).
[67] F. Thiel, I. Mualem, D. Meidan, E. Barkai, and D. A. Kessler, Phys. Rev. Res. **2**, 043107 (2020).
[68] B. Munsky, I. Nemenman, and G. Bel, J. Chem. Phys. **131**, 235103 (2009).
[69] G. Bel, B. Munsky, and I. Nemenman, Phys. Biol. **7**, 016003 (2009).
[70] T. Rotbart, S. Reuveni, and M. Urbakh, Phys. Rev. E **92**, 060101(R) (2015).
[71] C. P. Gomes, B. Selman, and H. Kautz, in *Proceedings of the Fifteenth National/Tenth Conference on Artificial Intelligence/Innovative Applications of Artificial Intelligence, AAAI '98/IAAI '98* (American Association for Artificial Intelligence, Washington, DC, 1998), pp. 431–437.
[72] C. P. Gomes, B. Selman, K. McAloon, and C. Tretkoff, in *Proceedings of the Fourth International Conference on Artificial Intelligence Planning Systems, AIPS'98* (AAAI Press, Washington, DC, 1998), pp. 208–213.
[73] O. L. Bonomo and A. Pal, Phys. Rev. E **103**, 052129 (2021).
[74] B. Misra and E. C. G. Sudarshan, J. Math. Phys. **18**, 756 (1977).
[75] I. S. Gradshteyn and I. M. Ryzhik, *Table of Integrals, Series, and Products*, 7th ed. (Elsevier/Academic Press, Amsterdam, 2007).
[76] X.-P. Xu, Eur. Phys. J. B **77**, 479 (2010).
[77] S. Omanakuttan and A. Lakshminarayan, Phys. Rev. E **103**, 012207 (2021).
[78] D. A. Kessler, E. Barkai, and K. Ziegler, Phys. Rev. A **103**, 022222 (2021).
[79] Our measure of first-detection is based on the number of measurements made, which for $w = 0$ is the measurement time divided by the fixed τ (neglecting fluctuations). For $w \neq 0$ one can also record the time until the first-detection, namely the sum of all the waiting times, until the first-detection.
[80] N. A. Mecholsky, S. Akhbarifar, W. Lutze, M. Brandys, and I. L. Pegg, Data in Brief **39**, 107508 (2021).
[81] F. W. J. Olver, A. B. Olde Daalhuis, D. W. Lozier, B. I. Schneider, R. F. Boisvert, C. W. Clark, B. R. Miller, B. V. Saunders, H. S. Cohl, and M. A. McClain, *NIST Digital Library of Mathematical Functions* (National Institute of Standards and Technology, Gaithersburg, MD, 2021).
[82] P. Jordan and E. Wigner, Z. Phys. **47**, 631 (1928).
[83] P. J. Salgado, L. Dagdug, and D. Boyer, Phys. Rev. E **109**, 024134 (2024).